Crystals 2022

MDPI

Type of the Paper (Proceedings)

Electronic structures of Eu-doped $FAPbI_3$ perovskite crystals studied by first-principles calculation

Atsushi Suzuki[1] and Takeo Oku[1]

[1] The University of Shiga Prefecture, 2500 Hassaka, Hikone, Shiga 522-8533, Japan; suzuki@mat.usp.ac.jp, oku@mat.usp.ac.jp

* Correspondence: suzuki@mat.usp.ac.jp; Tel.:+81-749-28-8369: (A. S.)

† Presented at the title, place, and date.

Abstract: Effects of maxed-valence states on electronic structures of europium (Eu)-incorporated $CH(NH_2)_2PbI_3$ ($FAPbI_3$) and $CH_3NH_3PbI_3$ ($MAPbI_3$) perovskite crystals were investigated by first-principles calculation. Partial replacements of europium ions into the perovskite crystal influenced the electronic structures. In the case of the $FAPb(Eu^{+3})I_3$ crystal, there was wide distribution of the 5p orbital of iodine near the valence band, and the 3d orbital of the Eu^{3+} ion near the conductive band. Incorporation of Eu^{2+} ion into the perovskite crystal provided a low energy levels at VB with increase of the band gap, and decrease of m_h^*/m_e. The behaviour expects improvement of carrier-mobility related to short circuit current and the conversion efficiency, as compared with incorporation of Eu^{3+} ion into the perovskite crystal. The partial substitution of europium ion at position of lead ion as B-site in the perovskite crystal caused the electron correlation based on the charge transfer between 5p orbital of iodine and 3d orbital of Eu ion, and narrowed the band dispersion with decrease of effective mass ratio, which expected to improve the carrier mobility related to the short circuit current density and the conversion efficiency.

Keywords: perovskite crystal; first-principles calculation; band structure; NMR

1. Introduction

The perovskite solar cells have a great advantage to develop the photovoltaic application using perovskite crystal varied with chemical element and crystal structure [1-3]. The perovskite solar cells have high performance of the photovoltaic properties. The wide-band gap perovskite tandem solar cell has been developed for practical use of photovoltaic devices [4, 5]. The photovoltaic properties were influenced by chemical elements and crystalline structure in active layer [6, 7]. The photovoltaic performance was based on optimization with tuning the band structure and the effective mass related with carrier mobility. For example, incorporation of alkali metal [8-10], organic cation [11, 12], transition metal [13-20], tin [21, 22] and halogen ions [23, 24] improved the photovoltaic performance. The decomposition was suppressed by partial substitution of formamidinium (FA) [25], guanidinium (GA), ethylammonium (EA) and alkali metal ions instead of methyl ammonium (MA) at the A-sites, and transition metals (copper [18, 19], cobalt [26] and nickel) incorporated to lead (Pb) ions at the B-sites into the $CH_3NH_3PbX_3$ ($MAPbX_3$) perovskite crystal, where X were the halogen ions. The surface modifications promoted the carrier diffusion with suppressing the deterioration.

The photovoltaic performances were associated with the electronic structure [27, 28]. Tolerance factor varied with effective ionic radii was used for predicting the thermodynamic stability of the crystal as cubic crystal system [29]. Transition metal-incorporated perovskite crystal had a high potential to improve the photovoltaic properties [30, 31]. Recently, the photovoltaic properties of lanthanide perovskite compounds were characterized by experimental results using first-principle calculation [32-35]. Rare-earth-based compound have unique type of physical phenomena as heavy-electron behaviour [36, 37]. The photovoltaic performance, the electronic structure and partial density of state were studied by the first-principle calculation using density functional theory (DFT) [38-41]. Partial replacement of

Citation: Lastname, F.; Lastname, F.; Lastname, F. Title. *Chem. Proc.* **2021**, *3*, x. https://doi.org/10.3390/xxxxx

Published: date

europium ion with B site in the perovskite crystal prevented the decomposition, improving the stability of the performance.

The purpose of the present study is to focus on improvement of the photovoltaic properties by investigating effects of europium in the $FAPbI_3$ perovskite crystal. The electronic structure of the Eu-incorporated $FAPbI_3$ perovskite crystal was predicted by first-principles calculation. The electronic structures, electron density distribution, band structure, partial density of state (pDOS), chemical shifts of ^{127}I-NMR, electronic field gradient (EFG) and asymmetric parameter (η) were considered in the Eu-incorporated $FAPbI_3$ or $MAPbI_3$ perovskite crystal. The photovoltaic mechanism was discussed by the electronic structure.

2. Calculation

The electronic structures of the perovskite crystals were single-point-calculated with crystallographic structural data obtained from X-ray diffraction patterns. The *ab initio* quantum calculations were performed using the Vanderbilt ultrasoft pseudo-potentials, scalar relativistic generalized gradient approximations and Perdew-Burke-Ernzerhof (GGA-PBE) exchange-correlation functional and density functional theory (DFT+U, U = 6.0 eV) (Quantum Espresso software). The basis-functions were used properly according to the cases of itinerant and localized electron system. Plane-wave basis set cut offs for the wave functions and charge density were set at 25 and 225 Rydberg (Ry). The perovskite crystals were constructed with experimental lattice constants (a = 6.362 Å) and crystal system (cubic $Pm\overline{3}m$) [41, 42]. Uniform k-point grid (4 × 4 × 4) in the Brillouin zone was used to calculate the electronic structure and partial density of state. The Eu-incorporated $FAPbI_3$ perovskite cubic crystals as models were constructed with the supercells (2 × 2 × 2) as initial unit cell, and were used for the band calculation. The band structures and effective mass were analysed for the Brillouin zone of the perovskite crystal along the direction of wave vector.

Path for $FAPbI_3$ perovskite crystal were set as follows, Γ (0, 0, 0)→X (0, ½, 0)→M (1/2, 1/2, 0)→Γ →R (1/2, 1/2, 1/2)→X, M→R. Pb cation was set at the position of Γ (0, 0, 0). FA cation was set in the centre position of unit cell (1 × 1 × 1). Path for the $FAPb(Eu)I_3$ perovskite crystals were set as follows, Γ (0, 0, 0)→X (1/2, 0, 1/2)→W (1/2, 1/4, 3/4)→K (3/8, 3/8, 3/4)→Γ→L (1/2, 1/2, 1/2)→U (5/8, 1/4, 5/8)→ W (1/2, 1/4, 3/4)→L→K|U→X. For minor partial replacement, Eu cation was replaced with Pb cation in the centre position of the supercell (2 × 2 × 2). The density of states (DOS) and partial density of states (pDOS) were calculated to make clear the energy level for each orbital near valence band (VB) and conduction band (CB). The chemical shifts of ^{127}I-NMR, ^{157}Eu-NMR, electronic field gradient (EFG) and asymmetry parameter (η) of the Eu-doped $MAPbI_3$ crystal were calculated by hybrid DFT using unrestricted B3LYP (UB3LYP) and GIAO with SSDall as the basis set (Gaussian 09).

3. Results and discussion

The band structure, partial density of state, electronic density distribution in the $FAPb(Eu^{+3})I_3$ perovskite crystal were calculated by first-principle calculation. The band structure and partial density of state (pDOS), the electronic density distribution in the $FAPb(Eu^{3+})I_3$ perovskite crystal are shown in Fig. 1(a). The energy levels at valence band and conduction band, band gap, effective mass ratio of electron and hole in the electron structure were calculated. The direct band gap was obtained to be 1.45 eV. The band dispersion curvature at wave vector near Γ (0, 0, 0) had the effective mass ratio of electron and hole to be 0.04 and 0.07. This result indicates that makes it is easy for carriers to diffuse in the crystal, improving the carrier mobility, short circuit current density and conversion efficiency. The partial density of state and enlarge view of 3p, 3d and 4f of Eu^{3+} in the $FAPb(Eu^{3+})I_3$ perovskite crystal were considered. The 5p orbital of iodine, 3d and p orbitals of Eu^{3+} were widely distributed near valence band state. Near the conduction band, 6p orbital of Pb, 3d and 4f orbitals of Eu^{3+} were widely distributed. The itinerant behaviour indicates a different tendency from the localized system of the $FAEuI_3$ perovskite crystal [39].

In the case of the $FAPb(Eu^{2+})I_3$ perovskite crystal, the band structure, and pDOS was considered as shown in Fig. 1(b). The band structure had the direct band gap of E_g of 1.53 eV near wave vector at Γ (0, 0, 0). The band dispersion curvature near at Γ (0, 0, 0) had the effective mass of electron and hole of 0.03 and 0.01, respectively. The itinerary characteristics indicates the light electronic system. The carriers are easy to diffuse with increase of mobility in the $FAPb(Eu^{2+})I_3$ perovskite crystal, as compared with those of the $FAPb(Eu^{3+})I_3$ perovskite crystal. The partial density of state and enlarged view of 3p, 3d and 4f orbitals of Eu^{2+} in the crystal are demonstrated. The 5p orbital of iodine, and 3d, 4f orbital of Eu^{2+} in the crystal were widely distributed. Near the conduction band, 6p orbital of Pb were distributed and increased. Incorporation of Eu^{2+} ion into the crystal did not influenced on the pDOS of 5p orbital of Pb and 5p orbital of iodine in the crystal. This behaviour expects a slight influence on the carrier mobility. The electronic behaviour expects the itinerant

characteristics with promotion of the carrier diffusion on the 5p orbital of I in the crystal structure. Incorporation of Eu^{2+} ion into the perovskite crystal provided a low energy levels at VB with increase of the band gap, and decrease of m_h^*/m_e. The behaviour expects improvement of carrier-mobility related to short circuit current and the conversion efficiency, as compared with incorporation of Eu^{3+} ion into the perovskite crystal.

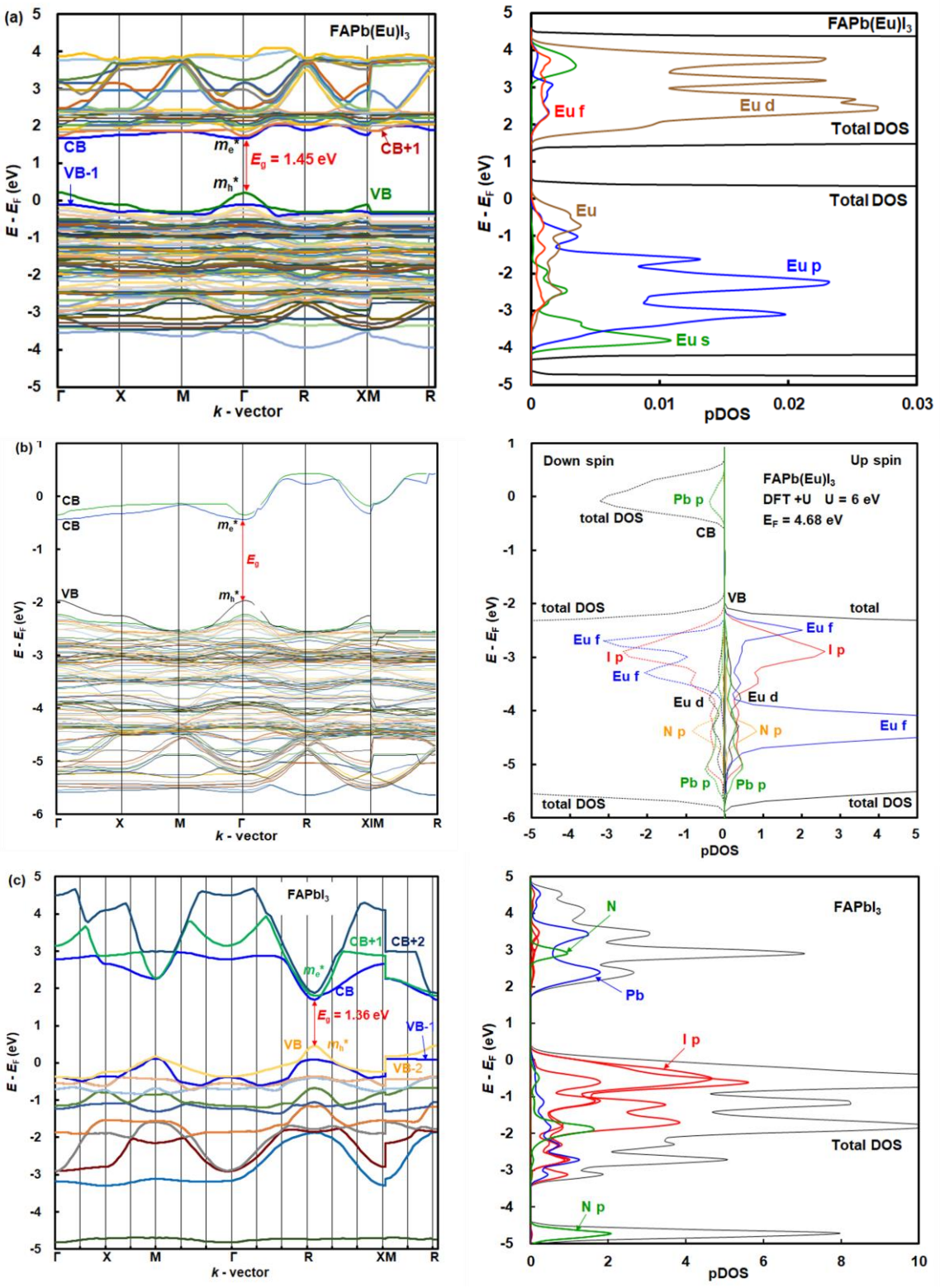

Figure 1. (a) Band structure, (b) density of state, and enlarged view of 3p, 3d, and 4f orbitals of Eu^{3+} in (a) $FAPb(Eu^{+3})I_3$ (b) $FAPb(Eu^{+2})I_3$ and the (c) $FAPbI_3$ crystals.

The chemical shifts of ^{127}I-NMR in the MAPb(Eu^{3+})I_3 rather than MAPb(Eu^{2+})I_3 were remarkably shifted by nuclear quadrupole interaction in proportion to extent of value in Q, EFG tensor and η. The chemical shifts of ^{127}I-NMR in the MAPb(Eu)I_3 perovskite crystal depend on extent of nuclear quadrupole interaction based on Q-tensor related with EFG and η of the iodine ligand with extent of spin-orbital interaction based on electron density distribution and hybrization of s, p and d orbital on the Eu ion in the coordinatin structure. The chemical shifts of ^{127}I-NMR of the MAPb(Eu^{3+})I_3 perovskite crystal were based on the anisotropic magnetic interaction between nearest neighbour ligand and Eu^{3+} ion in the coordination structure. In the case of the MAPb(Eu^{2+})I_3 perovskite crystal, the chemical shifts of ^{127}I-NMR expected the isotropic behavior with narrow splitting in the magnetic field. The isotropic magnetic interaction was derived from nuclear Zeeman interaction, isotropic hyperfine interaction between electron and nuclear spins, and nuclear quadrupole interaction based on EFG and η of the Eu^{2+} ion with slight extent of electron density distribution on the Eu-I band in the coordination structure.

The electronic correlation based on the charge transfer from 3d, 4f hybrid orbital of europium ion to 5p orbital of iodine ion as ligand determined the itinerary system with increase of the carrier mobility related to reciprocal of the effective mass of hole. The anisotropic behaviour were associated with the crystal field perturbation of energy level splitting and the nuclear quadruple interaction based on EFG and η. The itinerary behaviour would promote to increase the carrier mobility, predicting improvement of the short circuit current density. The valence fluctuation of Eu^{2+} and Eu^{3+} ions influence the charge transfer between metal and ligand in the perovskite crystal. The mechanisms have itinerant variation based on exchange interaction in the coordination structure. The electronic structures of the doping of lanthanide ions into $MAPbI_3$ perovskite crystals were considered. The electronic correlation with the crystal field perturbation expects the photovoltaic mechanism, improving the stability of conversion efficiency.

4. Conclusion

Partial replacement of Eu at the Pb site in the perovskite crystal influenced the electronic structure, the effective mass related to carrier mobility and E_g with energy level at VB state. In the case of the FAPb(Eu^{+3})I_3 crystal, 3d and 4f orbital of Eu ion appeared near VB, and 3d orbital was widely distributed near CB. The effective mass ratio was slightly increased by incorporation of Eu^{+3} ion. In the case of the FAPb(Eu^{+2})I_3 crystal, 4f orbitals of Eu^{+2} ion and 5p orbital of iodine ion were strongly appeared near VB, and 3d orbital of Eu^{2+} ion and 5p orbital on Pb ion were distributed near CB. Incorporation of Eu^{+2} ion into the crystal decreased the effective mass ratio, promoting the career diffusion related to the mobility, expecting for improvement of the short circuit current density and conversion efficiency. The chemical shifts of ^{127}I-NMR of the MAPb(Eu^{2+})I_3 crystal depended on the extent of the nuclear quadrupole interaction based on EFG and η in the coordination structure. The electronic correlation promoted the charge transfer, improving the short circuit current density and conversion efficiency.

Author Contributions: Conceptualization, A.S.; methodology, A.S.; software, A.S.; validation, A.S.; formal analysis, A.S.; investigation, A.S.; resources, A.S.; data curation, A.S.; writing—original draft preparation, A.S.; writing—review and editing, A.S., T.O.; visualization, A.S.; supervision, T.O.; project administration, T.O.; funding acquisition, A.S., T.O.

Funding: This research was supported by JSPS KAKENHI Grant Number JP 21K05261.

Conflicts of Interest: The authors declare no conflict of interest.

References

1. Dunfield S.P.; Bliss L.; Zhang F.; Luther J.M.; Zhu K.; Hest M.F.A. M.; Reese M.O.; Berry J.J., From defects to degradation: A mechanistic understanding of degradation in perovskite solar cell devices and modules, *Adv. Energy Mater.* **2020**, *10*, 1904054. DOI: 10.1002/aenm.201904054
2. Jeong M.; Choi I.W.; Go E.M.; Cho Y.; Kim M.; Lee B.; Jeong S.; Jo Y.; Choi H.W.; Lee J.; Bae J.H.; Kwak S.K.; Kim D.S.; Yang C., Stable perovskite solar cells with efficiency exceeding 24.8% and 0.3-V voltage loss, *Science* **2020**, *369*, 1615-1620. DOI: 10.1126/science.abb7167

3. Yang Z.; Yu Z.; Wei H.; Xiao X.; Ni Z.; Chen B.; Deng Y.; Habisreutinger S.N.; Chen X.; Wang K.; Zhao J.; Rudd P.N.; Berry J.J.; Beard M.C.; Huang J., Enhancing electron diffusion length in narrow-bandgap perovskites for efficient monolithic perovskite tandem solar cells, *Nat. Commun.* **2019**, *10*, 4498. https://doi.org/10.1038/s41467-019-12513-x
4. Li Z.; Kim T.H.; Han S.Y.; Yun Y.J.; Jeong S.; Jo B.; Ok S.A.; Yim W.; Lee S.H.; Kim K.; Moon S.; Park J.Y.; Ahn T.K.; Lee H.S.J.; Park H.J., Wide-bandgap perovskite/gallium arsenide tandem solar cells, *Adv. Energy Mater.* **2020**, *10*, 1903085. https://doi.org/10.1002/aenm.201903085
5. Kim D.; Jung H.J.; Park I.J.; Larson B.W.; Dunfield S.P.; Xiao C.; Kim J.; Tong J.; Boonmongkolras P.; Ji S.G.; Zhang F.; Pae S.R.; Kim M.; Kang S.B.; Dravid V.; Berry J.J.; Kim J.Y.; Zhu K.; Kim D.H.; Shin B., Efficient, stable silicon tandem cells enabled by anion-engineered wide-bandgap perovskites, *Science* **2020**, *368*, 155–160. DOI: 10.1126/science.aba3433
6. McMeekin D.P.; Sadoughi G.; Rehman W.; Eperon G.E.; Saliba M.; Hörantner M.T.; Haghighirad A.; Sakai N.; Korte L.; Rech B.; Johnston M.B.; Herz L.M.; Snaith H.J., A mixed-cation lead mixed-halide perovskite absorber for tandem solar cells, *Science* **2016**, *351*, 151-155. DOI: 10.1126/science.aad5845
7. Kishimoto T.; Suzuki A.; Ueoka N.; Oku T., Effects of guanidinium addition to $CH_3NH_3PbI_{3-x}Cl_x$ perovskite photovoltaic devices, *J. Ceram. Soc. Jpn.* **2019**, *127*, 491-497. https://doi.org/10.2109/jcersj2.18214
8. Wang Y.; Dar M.I.; Ono L.K.; Zhang T.; Kan M.; Li Y.; Zhang L.; Wang X.; Yang Y.; Gao X.; Qi Y.; Grätzel M.; Zhao Y., Thermodynamically stabilized β-$CsPbI_3$–based perovskite solar cells with efficiencies >18%, *Science* **2019**, *365*, 591-595. DOI: 10.1126/science.aav8680
9. Chen Y.; Li N.; Wang L.; Li L.; Xu Z.; Jiao H.; Liu P.; Zhu C.; Zai H.; Sun M.; Zou W.; Zhang S.; Xing G.; Liu X.; Wang J.; Li D.; Huang B.; Chen Q.; Zhou H., Impacts of alkaline on the defects property and crystallization kinetics in perovskite solar cells, *Nat. Commun.* **2019**, *10*, 1112. https://doi.org/10.1038/s41467-019-09093-1
10. Oku T.; Kandori S.; Taguchi M.; Suzuki A.; Okita M.; Minami S.; Fukunishi S.; Tachikawa T., Polysilane-inserted methylammonium lead iodide perovskite solar cells doped with formamidinium and potassium, *Energies* **2020**, *13*, 4776. https://doi.org/10.3390/en13184776
11. Jodlowski A.D.; Carmona C.R.; Grancini G.; Salado M.; Ralaiarisoa M.; Ahmad S.; Koch N.; Camacho L.; Miguel G.; Nazeeruddin M.K., Large guanidinium cation mixed with methylammonium in lead iodide perovskites for 19% efficient solar cells, *Nat. Energy* **2017**, *2*, 972-979. https://doi.org/10.1038/s41560-017-0054-3
12. Saidaminov M.I.; Kim J.; Jain A.; Bermudez R.Q.; Tan H.; Long G.; Tan F.; Johnston A.; Zhao Y.; Voznyy O.; Sargent E. H., Suppression of atomic vacancies via incorporation of isovalent small ions to increase the stability of halide perovskite solar cells in ambient air, *Nat. Energy* **2018**, *3*, 648-654. https://doi.org/10.1038/s41560-018-0192-2
13. Gong X.; Guan L.; Pan H.; Sun Q.; Zhao X.; Li H.; Pan H.; Shen Y.; Shao Y.; Sun L.; Cui Z.; Ding L.; Wang M., Highly efficient perovskite solar cells via nickel passivation, *Adv. Functional Mater.* **2018**, *28*, 1804286. https://doi.org/10.1002/adfm.201804286
14. Zheng H.; Liu G.; Xu X.; Alsaedi A.; Hayat T.; Pan X.; Dai S., Acquiring high-performance and stable mixed-dimensional perovskite solar cells by using a transition-metal-substituted Pb precursor, *ChemSusChem* **2018**, *11*, 3269-3275. https://doi.org/10.1002/cssc.201801171
15. Suzuki A.; Oku T., Effects of transition metals incorporated into perovskite crystals on the electronic structures and magnetic properties by first-principles calculation, *Heliyon* **2018**, *4*, e00755. https://doi.org/10.1016/j.heliyon.2018.e00755
16. Kooijman A.; Muscarella L.A.; Williams R.M., Perovskite thin film materials stabilized and enhanced by Zinc(II) doping, *Appl. Sci.* **2019**, *9*, 1678. https://doi.org/10.3390/app9081678
17. Zhu H.X.; Wang X.H.; Zhuang G.C., Electronic structure, magnetism properties and optical absorption of organometal halide perovskite $CH_3NH_3XI_3$ (X = Fe, Mn), *Applied Physics A* **2019**, *125*, 45. https://doi.org/10.1007/s00339-018-2347-1
18. Ueoka N.; Oku T.; Suzuki A., Additive effects of alkali metals on Cu-modified $CH_3NH_3PbI_{3-\delta}Cl_\delta$ photovoltaic devices, *RSC Adv.* **2019**, *9*, 24231. DOI: 10.1039/c9ra03068a
19. Suzuki A.; Kitagawa K.; Oku T.; Okita M.; Fukunishi S.; Tachikawa T., Additive effects of copper and alkali metal halides into methylammonium lead iodide perovskite solar cells, *Electron. Mater. Lett.* **2021**, https://doi.org/10.1007/s13391-021-00325-5
20. Wang K.L.; Wang R.; Wang Z.K.; Li M.; Zhang Y.; Ma H.; Liao L.S.; Yang Y., Tailored phase transformation of $CsPbI_2Br$ films by copper(II) bromide for high-performance all-inorganic perovskite solar cells, *Nano Lett.* **2019**, *19*, 5176. https://doi.org/10.1021/acs.nanolett.9b01553
21. Ueoka N.; Oku T., Effects of co-addition of sodium chloride and copper(II) bromide to mixed-cation mixed-halide perovskite photovoltaic devices, *ACS Appl. Energy Mater.* **2020**, *3*, 7272-7283. https://dx.doi.org/10.1021/acsaem.0c00182
22. Tong J.; Song Z.; Kim D.H.; Chen X.; Chen C.; Palmstrom A.F.; Ndione P.F.; Reese1 M.O.; Dunfield S.P.; Reid O.G.; Liu J.; Zhang F.; Harvey S.P.; Li Z.; Christensen S.T.; Teeter G.; Zhao D.; Jassim M.M.A.; Hest M.F.A.M.; Beard M.C.; Shaheen S. E.; Berry J.J.; Yan Y.; Zhu K., Carrier lifetimes of >1 μs in Sn-Pb perovskites enable efficient all-perovskite tandem solar cells, *Science* **2019**, *364*, 475-479. DOI: 10.1126/science.aav7911
23. Peng L.; Xie W., Theoretical and experimental investigations on the bulk photovoltaic effect in lead-free perovskites $MASnI_3$ and $FASnI_3$, *RSC Adv.*, **2020**, *10*, 14679-14688. DOI: 10.1039/D0RA02584D
24. Suzuki A.; Kato M.; Ueoka N.; Oku T., Additive effect of formamidinium chloride in methylammonium lead halide compound-based perovskite solar cells, *J. Electron. Mater.* **2019**, *48*, 3900-3907. https://doi.org/10.1007/s11664-019-07153-2

25. Li N.; Tao S.; Chen Y.; Niu X.; Onwudinanti C.K.; Hu C.; Qiu Z.; Xu Z.; Zheng G.; Wang L.; Zhang Y.; Li L.; Liu H.; Lun Y.; Hong J.; Wang X.; Liu Y.; Xie H.; Gao Y.; Bai Y.; Yang S.; Brocks G.; Chen Q.; Zhou H., Cation and anion immobilization through chemical bonding enhancement with fluorides for stable halide perovskite solar cells, *Nature Energy* **2019**, *4*, 408–415. https://doi.org/10.1038/s41560-019-0382-6
26. Xu W.; Zheng L.; Zhang X.; Cao Y.; Meng T.; Wu D.; Liu L.; Hu W.; Gong X., Efficient perovskite solar cells fabricated by Co partially substituted hybrid perovskite, *Adv. Energy Mater.* **2018**, *8*, 1703178. https://doi.org/10.1002/aenm.201703178
27. Suzuki A.; Oku T., First-principles calculation study of electronic structures of alkali metals (Li, K, Na and Rb)-incorporated formamidinium lead halide perovskite compounds, *Appl. Surf. Sci.* **2019**, *483*, 912-921. https://doi.org/10.1016/j.apsusc.2019.04.049
28. Suzuki A.; Miyamoto Y.; Oku T., Electronic structures, spectroscopic properties, and thermodynamic characterization of sodium- or potassium-incorporated $CH_3NH_3PbI_3$ by first-principles calculation *J. Mater. Sci.* **2020**, *55*, 9728–9738. https://doi.org/10.1007/s10853-020-04511-y
29. Oku T., Crystal structures of perovskite halide compounds used for solar cells, *Rev. Adv. Mater. Sci.* **2020**, *59*, 264-305. https://doi.org/10.1515/rams-2020-0015
30. Suzuki A.; Oku T., Electronic structures and magnetic properties of transition metal doped $CsPbI_3$ perovskite compounds by first-principles calculation, *Phys. Solid State*, **2019**, *61*, 1074–1085. https://doi.org/10.1134/S1063783419060258
31. Suzuki A.; Oe M.; Oku T., Fabrication and characterization of Ni-, Co-, and Rb-incorporated $CH_3NH_3PbI_3$ perovskite solar cells, *J. Electronic Mater.* **2021**, *50*, 1980-1995. https://doi.org/10.1007/s11664-021-08759-1
32. Pazoki M.; Edvinsson T., Metal replacement in perovskite solar cell materials: chemical bonding effects and optoelectronic properties, *Sustainable Energy Fuels*, **2018**, *2*, 1430-1445. https://doi.org/10.1039/C8SE00143J
33. Wang L.; Zhou H.; Hu J.; Huang B.; Sun M.; Dong B.; Zheng G.; Huang Y.; Chen Y.; Li L.; Xu Z.; Li N.; Liu Z.; Chen Q.; Sun L.D.; Yan C.H., A Eu^{3+}-Eu^{2+} ion redox shuttle imparts operational durability to Pb-I perovskite solar cells, *Science*, **2019**, *363*, 265-270. DOI: 10.1126/science.aau5701
34. Bala A.; Kumar V., Stability of the Eu^{2+} dopant in $CsPbBr_3$ perovskites: A first-principles study, *J. Phys. Chem.* C **2019**, *123*, 6965–6969. https://doi.org/10.1021/acs.jpcc.8b10261
35. Tian J.; Xue Q.; Yao Q.; Li N.; Brabec C. J.; Yip H.L., Inorganic halide perovskite solar cells: Progress and challenges, *Adv. Energy Mater.* **2020**, *10*, 2000183. https://doi.org/10.1002/aenm.202000183
36. Chen Y.; Liu S.; Zhou N.; Li N.; Zhou H.; Sun L.D.; Yan C.H., An overview of rare earth coupled lead halide perovskite and its application in photovoltaics and light emitting devices, *Prog. Mater. Sci.* **2020**, *18*, 100737. https://doi.org/10.1016/j.pmatsci.2020.100737
37. Yang S.; Zhao H.; Han Y.; Duan C.; Liu Z.; Liu S.F., Europium and acetate Co-doping strategy for developing stable and efficient $CsPbI_2Br$ perovskite solar cells, *Small*, **2019**, *15*, 1904387. https://doi.org/10.1002/smll.201904387
38. Song Z.; Xu W.; Wu Y.; Liu S.; Bi W.; Chen X.; Song H., Incorporating of lanthanides ions into perovskite film for efficient and stable perovskite solar cells, *Small*, **2020**, *16*, 2001770. https://doi.org/10.1002/smll.202001770
39. Pazoki M.; Röckert A.; Wolf M.J.; Imani R.; Edvinsson T.; Kullgren J., Electronic structure of organic–inorganic lanthanide iodide perovskite solar cell materials, *J. Mater. Chem.* A, **2017**, *5*, 23131-23138. https://doi.org/10.1039/C7TA07716E
40. Suzuki A.; Oku T., Effects of mixed-valence states of Eu-doped $FAPbI_3$ perovskite crystals studied by first-principles calculation, *Mater. Adv.*, **2021**, 2, 2609-2616. https://doi.org/10.1039/D0MA00994F
41. Weller M.T.; Weber O.J.; Frost J.M.; Walsh A., Cubic perovskite structure of black formamidinium lead iodide, α-$[HC(NH_2)_2]PbI_3$, at 298 K, *J. Phys. Chem. Lett.* **2015**, *6*, 3209-3212. https://doi.org/10.1021/acs.jpclett.5b01432
42. Mashiyama H.; Kurihara Y.; Azetsu T., Disordered cubic perovskite structure of $CH_3NH_3PbX_3$ (X = Cl, Br, I), *J. Korean Phys. Soc.* **1998**, *32*, S156–S158